Supplementary Information for

3D macroporous electrode and high-performance in lithium-ion batteries using SnO_2 coated on Cu foam

Ji Hyun Um[1,2], Myounggeun Choi[3], Hyeji Park[3], Yong-Hun Cho[4], David C. Dunand[5], Heeman Choe[3] & Yung-Eun Sung[1,2]

[1]School of Chemical and Biological Engineering, Seoul National University, Seoul 151-742, Republic of Korea

[2]Center for Nanoparticle Research, Institute for Basic Science (IBS), Seoul 151-742, Republic of Korea

[3]School of Advanced Materials Engineering, Kookmin University, Seoul 136-702, Republic of Korea

[4]Department of Chemical Engineering, Kangwon National University, Samcheok 245-711, Republic of Korea

[5]Department of Materials Science and Engineering, Northwestern University, Evanston, IL 60208, USA

Correspondence and requests for materials should be addressed to Y.-H. C. (email: yhun00@ kangwon.ac.kr) or to Y.-E. S. (email: ysung@snu.ac.kr)

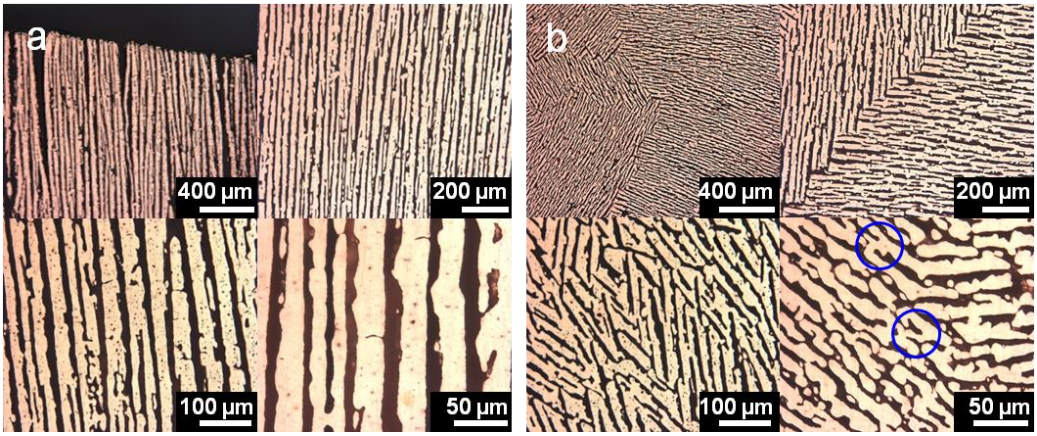

Supplementary Figure S1 Optical microscopic images of a polished Cu foam, after being cut either (a) vertically or (b) horizontally. The blue circles indicate lamellar bridges crossing the gaps between adjacent lamellae.

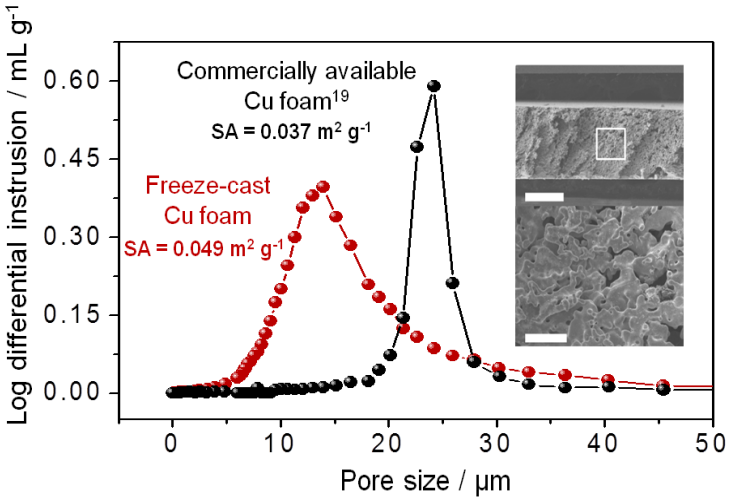

Supplementary Figure S2 Pore size distributions of commercially available Cu foam applied to previous our work and freeze-cast Cu foam used in this work. The inset shows a cross-sectional SEM image of Cu foam via freeze-casting (top) and an enlarged SEM image of the region indicated by white rectangle in top image (bottom). Scale bars, 400 μm and 40 μm.

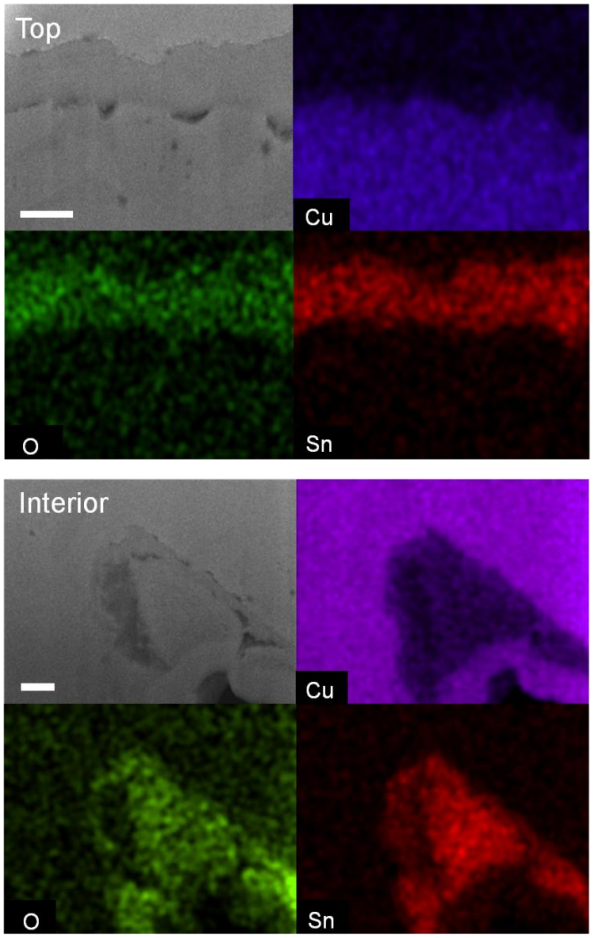

Supplementary Figure S3 Cross-sectional SEM and EDX images of SnO_2/Cu foam at top and interior regions with element mapping of Cu, O, and Sn, respectively. Scale bars, 500 nm (top) and 500 nm (interior).

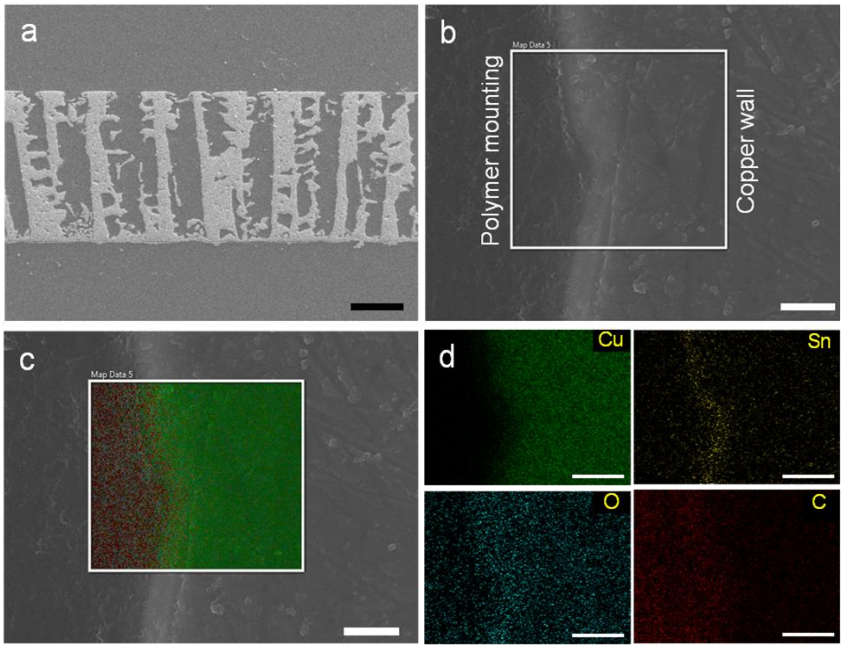

Supplementary Figure S4 (a) An entire cross-sectional SEM image of SnO_2/Cu foam. Scale bar, 100 µm. (b) SEM image of the magnified surface on lamella in SnO_2/Cu foam interior. Scale bar, 500 µm. (c) EDX mapping image of (b). Scale bar, 500 µm. (d) Element distribution of Cu, Sn, O, and C, respectively. Scale bar, 500 µm.

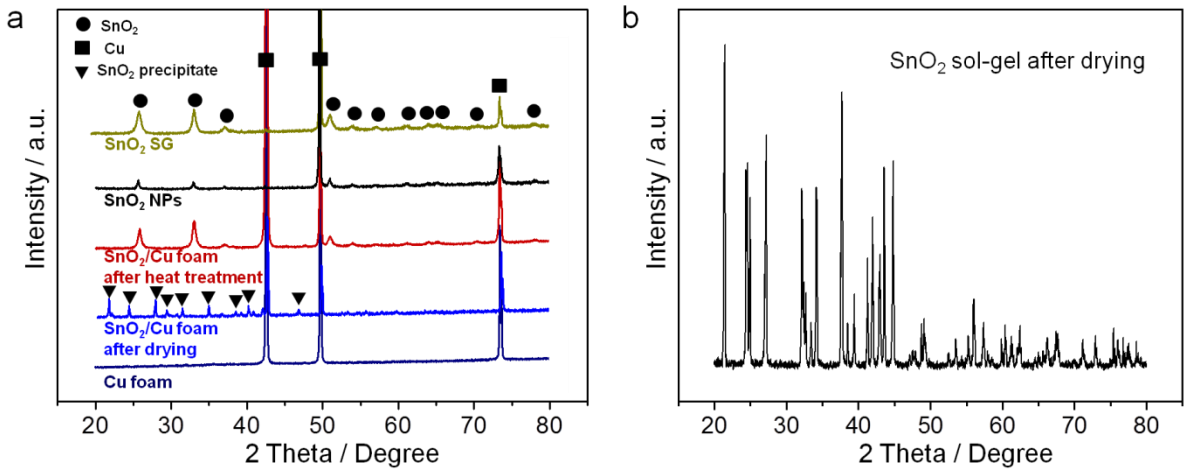

Supplementary Figure S5 (a) XRD patterns of pristine Cu foam, SnO_2/Cu foam after drying and heat treat ment, SnO_2 NPs, and SnO_2 SG. (b) XRD pattern of SnO_2 sol-gel precipitate. There are no oxidation peaks such as CuO and Cu_2O in the dried SnO_2/Cu foam. Only Cu and SnO_2 precipitate peaks resulted from the gelation and dehydration of SnO_2 sol are observed.

Details on stability evaluation in oxidation of the 3D Cu foam

In both electrodes of the dried SnO_2/Cu foam and the annealed SnO_2/Cu foam, the copper oxides (CuO and Cu_2O) being possibly formed through wet synthesis route such as sol-gel, were not observed from XRD analysis as shown in Supplementary Fig. S5. However, due to the detection limitation of XRD analysis, trace of the CuO and Cu_2O could be developed in the SnO_2/Cu foam electrode. Therefore, XPS analysis was conducted to examine the surface of Cu foam in the annealed SnO_2/Cu foam as the final product.

I. CuO

The XPS profile of annealed SnO_2/Cu foam is presented in Supplementary Fig. S5c. The two peaks located at around 934.9 eV and 954.8 eV are assigned to the binding energy of Cu $2p_{3/2}$ and Cu $2p_{1/2}$, respectively, which indicates the presence of Cu^{2+} (CuO) in the SnO_2/Cu foam. In addition, the shake-up satellite peak at a binding energy approximately 9 eV higher than that of Cu$2p_{3/2}$ further confirms the existence of the Cu^{2+} on the surface of SnO_2/Cu foam[R1,2]. XPS depth profiles with Ar ion beam etching were used to further probe the chemical oxidation state of SnO_2/Cu foam. The surface oxide layer of CuO is not detected after Ar ion etching after from 10 s to 120 s, confirming that the Cu foam maintains the metallic character under the thin surface oxide layer after the SnO_2 sol-gel coating.

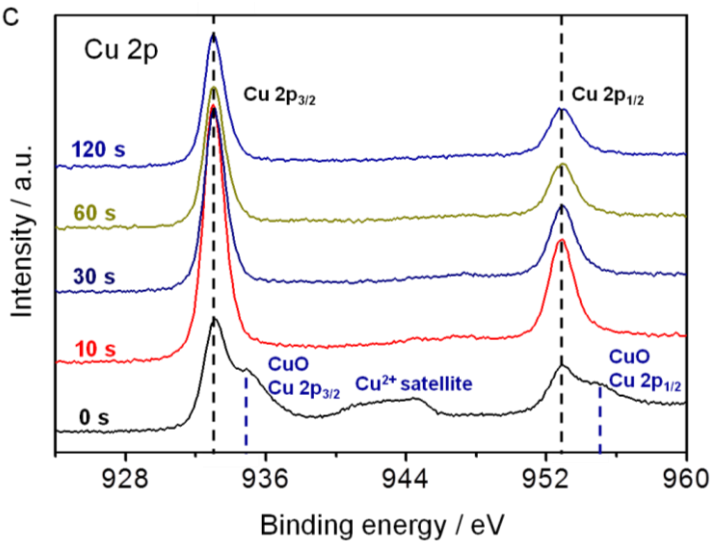

Supplementary Figure S5 (c) XPS profiles of SnO_2/Cu foam with various Ar ion etching time.

By using the XPS analysis operating condition (240 keV, 1 μA, and 2 x 2 mm^2) and the below equation, the etching rate could be estimated[R3,4].

$$\frac{z}{t} = \frac{M_w}{\rho\, n_A e}\, S j_P$$

M_w = Molar weight of the target [g/mol]
ρ = Density of material [g/cm^3]
n_A = Avogadro number [mol^{-1}]
e = Electron charge [A·s]
S = Sputtering yield
j_P = Primary ion current density [A/cm^2]

$$\frac{z}{t} = \left(\frac{63.5\ g}{mol}\right) x \left(\frac{cm^3}{8.96\ g}\right) x \left(\frac{mol}{6.02 \times 10^{23}}\right) x \left(\frac{1}{1.6 \times 10^{-19}\ A \cdot s}\right) x\ (6)^{*} x \left(\frac{0.25 \times 10^{-4}\ A}{cm^2}\right)$$

* The sputtering yield of copper at 240 keV can be estimated about 6 from the paper[R5].

The etching rate is calculated at 1.104 Å/s
And, the thickness of CuO during 10 s is about 1.1 nm.

The volume of CuO on the Cu foam can be estimated by using the surface area of Cu foam** and the thickness of CuO layer.
** The surface area could be calculated the specific surface area and the mass of Cu foam.

$$V_{CuO} = A_{Cu\ foam} \times z_{CuO} = \left(\frac{0.049\ m^2}{g}\right) \times (0.07554\ g) \times (1.1 \times 10^{-9}\ m)$$

From the 0.00407×10^{-9} m^3 of V_{CuO} and the 6.315 g/cm^3 of ρ_{CuO}, the mass of CuO on Cu foam is calculated at 0.0000257 g in the SnO_2/Cu foam electrode.

II. Cu_2O

In the case of Cu_2O, distinguishing it from metallic Cu in same XPS pattern is not easy due to the negligible difference of 0.2 eV between $Cu2p_{3/2}$ binding energies of Cu_2O and Cu[R6].

Although the quantitative analysis of Cu_2O through XPS analysis is difficult, by using XRD detection limitation (2~3 wt% with laboratory X-ray source and 0.1 wt% with synchrotron radiation source)[R7], approximately 3 wt% of the sample not observed in XRD pattern may be exist to maximum value in the SnO_2/Cu foam. When the mass of sample for XRD analysis is 0.002336 g, about 0.0000701 g of Cu_2O is in the SnO_2/Cu foam electrode.

The mass contribution of CuO and Cu_2O in total active material is approximately 2 wt% and 5 wt%, respectively.

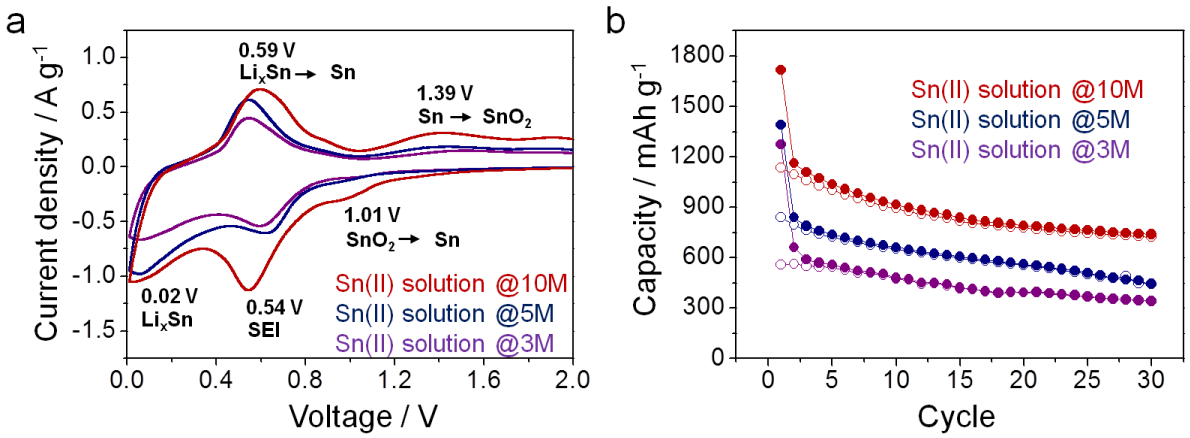

Supplementary Figure S6 (a) Cyclic voltammograms of SnO_2/Cu foam obtained from different sol concentration at a scan rate of 0.1 mV s^{-1}. (b) Cycle performance at current rate of 1 C.

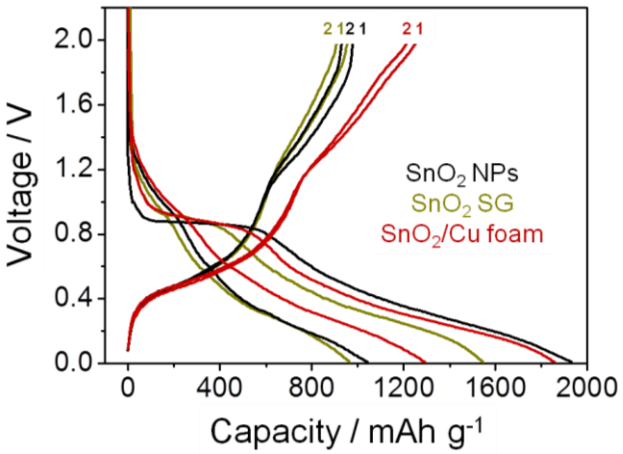

Supplementary Figure S7 Voltage profiles of SnO_2/Cu foam, SnO_2 SGP, and SnO_2 NPs during the first two cycles at 0.5 C.

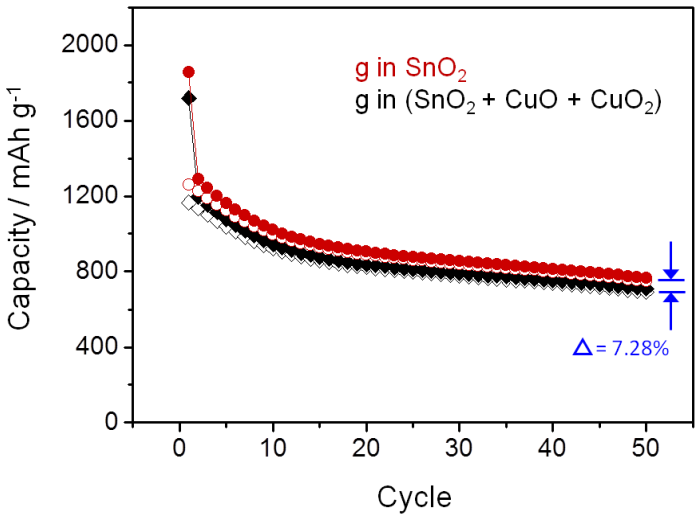

Supplementary Figure S8 Performance comparison of SnO_2/Cu foam with consideration of surface oxidation of Cu foam.

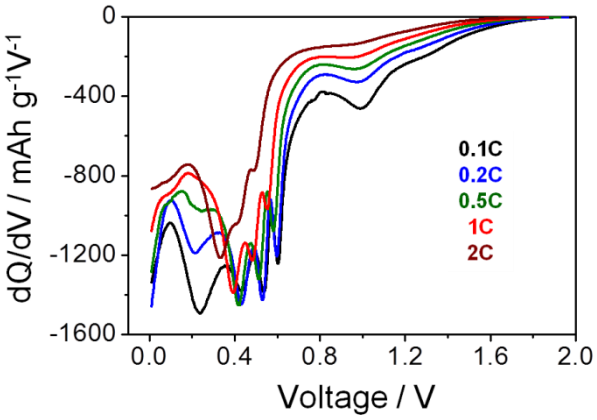

Supplementary Figure S9 Differential capacity profiles of SnO_2/Cu foam differentiated from the final discharge voltage profile (Fig. 4d) in each current rate step.

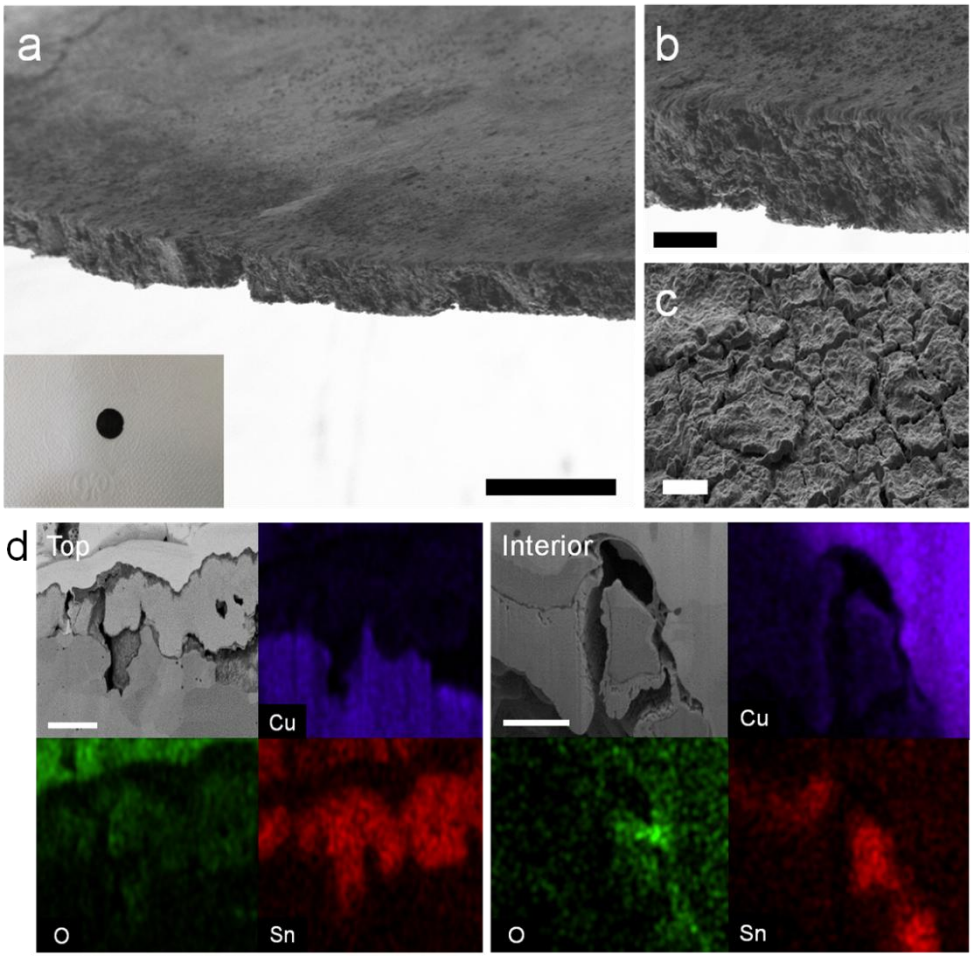

Supplementary Figure S10 (a) SEM image of SnO_2/Cu foam after 50 cycles at 0.5 C. Scale bar, 400 μm. The inset shows the photograph of disassembled SnO_2/Cu foam electrode. (b) Side view and (c) Top view SEM images of the SnO_2/Cu foam. Scale bars, 80 μm (Side view) and 8 μm (Top view). (d) Cross-sectional SEM and EDX images of SnO_2/Cu foam after 50 cycles at 1 C at top and interior regions with element mapping of Cu, O, and Sn, respectively. Scale bars, 2 μm (top) and 1 μm (interior).

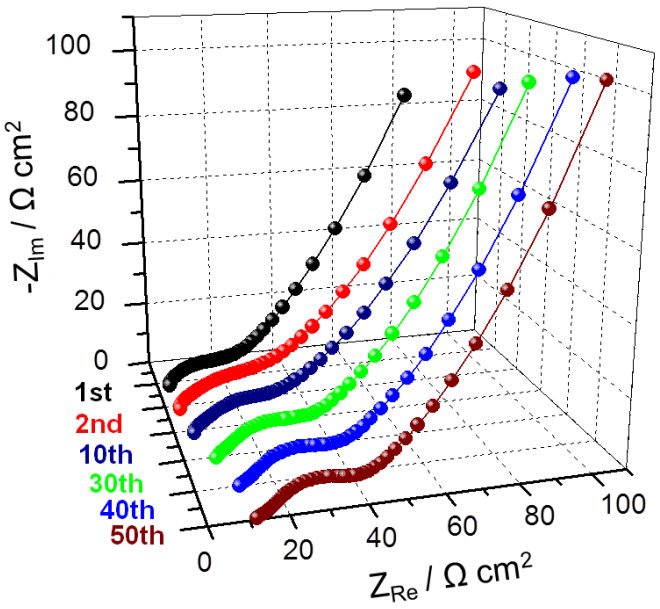

Supplementary Figure S11 Cell impedance tests of SnO_2/Cu foam after the selected cycles at 1 C.

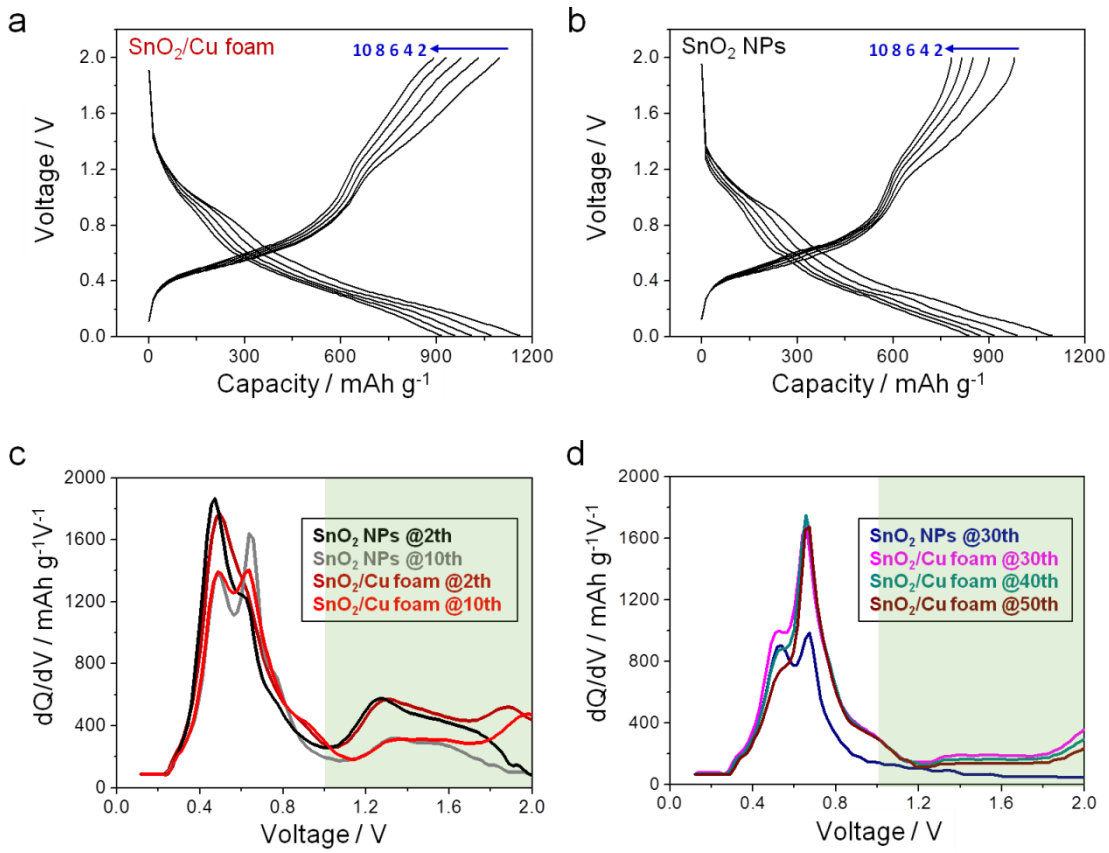

Supplementary Figure S12 Voltage profiles of (a) SnO_2/Cu foam and (b) SnO_2 NPs after the selected cycles at 1 C. Differential capacity profiles of the SnO_2/Cu foam and SnO_2 NPs differentiated from the charge voltage profiles in (c) the initial period (2th and 10th cycles) and (d) the late period (30th, 40th, and 50th cycles).

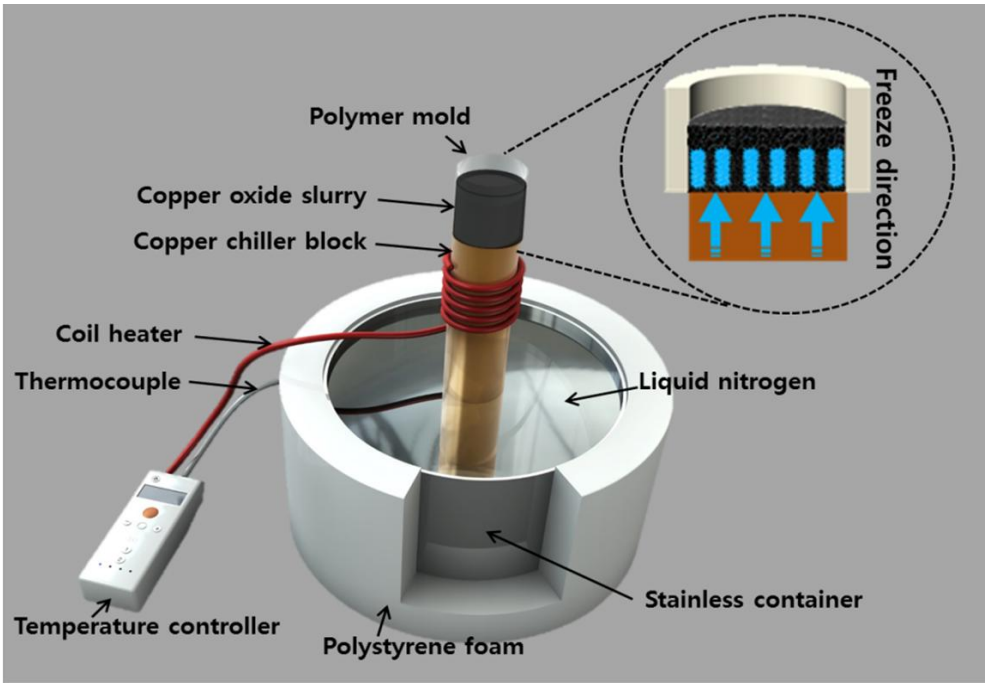

Supplementary Figure S13 Schematic diagram of a freeze-casting apparatus.

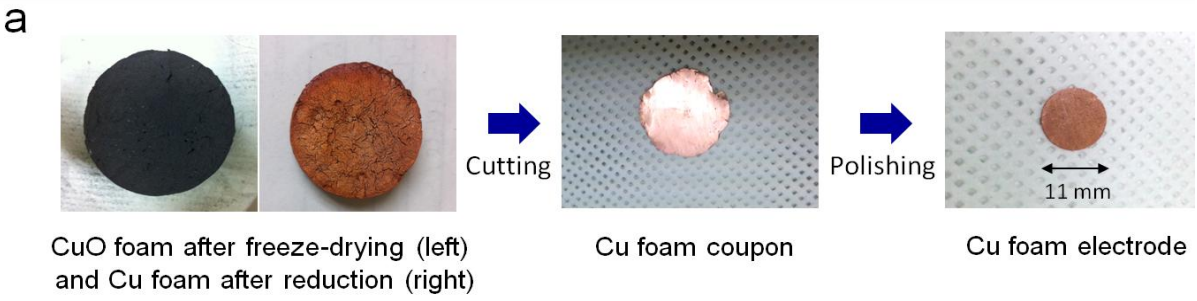

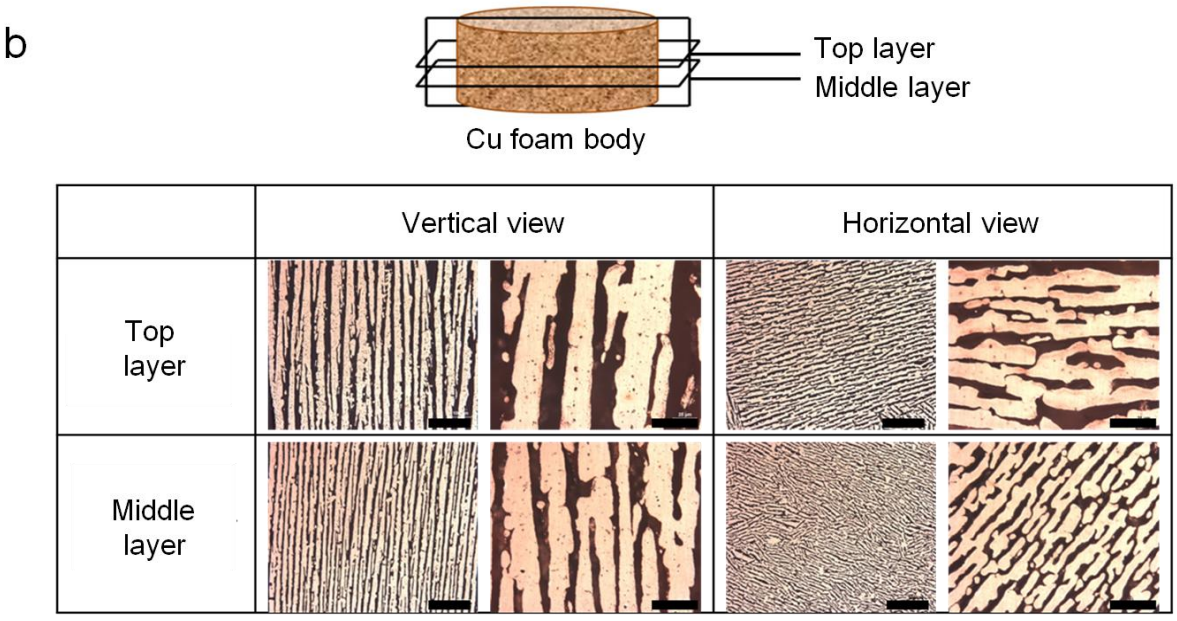

Supplementary Figure S14 (a) Photographs of manufacturing process from CuO foam body to Cu foam electrode. (b) Optical microscopic images of the Cu foam electrode at top and middle positions. Scale bars, 200 μm (left) and 50 μm (right) in each individual space of a table.

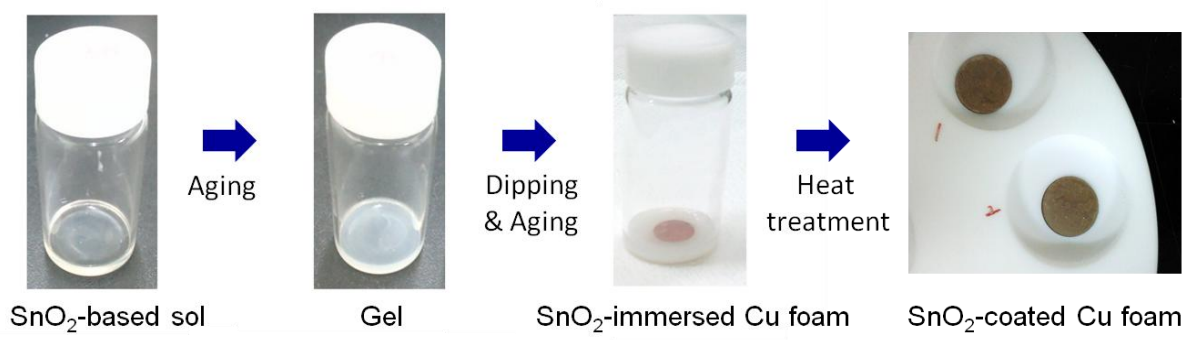

Supplementary Figure S15 Photographs of SnO_2 sol-gel coating process.

R1. Yin, M. *et al.* Copper Oxide Nanocrystals. *J. Am. Chem. Soc.* **127**, 9506-9511 (2005).

R2. Sakai, Y., Ninomiya, S. & Hiraoka, K. XPS depth analysis of CuO by electrospray droplet impact. *Surf. Interface Anal.* **44**, 938–941 (2012).

R3. Smentkowski, V. S. Trends in sputtering. *Progress in Surf. Sci.* **64**, 1-58 (2000).

R4. Behrisch, R. & Wittmaack, K. *et al.* Sputtering by Particle Bombardment I, II and III. Springer Series 560, Topics in Applied Physics, Vol 47, 52 and 64 (Springer-Verlag Berlin Heidelberg, 1981, 1983 and 1991).

R5. Sigmund, P. Sputtering Yield of Amorphous and Polycrystalline Targets. *Phys. Rev.* **184**, 383–416 (1969).

R6. Poulston, S., Marlet, P. M., Stone, P. & Bowker, M. Surface Oxidation and Reduction of CuO and Cu_2O Studied Using XPS and XAES. *Surf. Interface Anal.* **24**, 811-820 (1996).

R7. Drowley, C. I. 1-Application of Materials Characterization Techniques to Silicon Epitaxial Growth (ed. Strausser, Y.) 30 (Butterworth Heinemann, 1993).